CRYSTAL GROWTH & DESIGN
2008
VOL. 8, NO. 9
3285–3289

Large-Scale Synthesis of In_2O_3 Nanocubes Under Nondynamic Equilibrium Model

Youguo Yan,*,† Lixia Zhou,† Ye Zhang,‡ Jun Zhang,† and Songqing Hu†

College of Physical Science and Technology, China University of Petroleum, 257061 Dongying, Shandong, P. R. China, and Key Laboratory of Materials Physics, Anhui Key Laboratory of Nanomaterials and Nanotechnology, Institute of Solid State Physics, Chinese Academy of Sciences, P.O. Box 1129, 230031 Hefei, Anhui, P. R. China

Received January 28, 2008; Revised Manuscript Received April 30, 2008

ABSTRACT: Large-scale synthesis of In_2O_3 nanocubes was realized by modulating experimental parameters including the heating and depositing temperatures through the chemical vapor deposition (CVD) method. The configuration of In_2O_3 nanocubes indicated that the growth was isotropic along three equivalent crystallographic directions [100]. A nondynamic equilibrium growth model was proposed to explain the formation of In_2O_3 nanocubes combined with two contrastive experiments. These two experiments indicated that the formation of nanocubes depended on two crucial factors: relatively low growth temperature and high supersaturation ratio. The dynamic growth process is discussed in depth. The research results may not only facilitate the exploration of new approaches of preparing various nanostructures for potential technical applications but also give a deeper understanding of the fundamental physical and chemical processes of CVD methods.

1. Introduction

Semiconducting metal oxides as chemical sensing materials have been extensively studied for a long time due to their advantageous features, such as good sensitivity to ambient conditions and simplicity in fabrication.[1–3] Among them, low-dimensional In_2O_3 materials have been found to have a pronounced sensitivity to gases, for example, O_3, Cl_2, NO_2, NH_3, CO, H_2, and other species.[4–15]

In theory, large surface-to-volume ratios and high surface activity are two main factors determining the sensitivity of chemical sensors. Thus, the synthesis of small-sized nanoparticles terminated with high energy planes is an effective route to improve the sensitivity of chemical sensors. As for In_2O_3 particles, the sensitivity is related to its size and exposed crystalline planes. Generally, the obtained In_2O_3 particles are terminated with low energy planes (111) under kinetic equilibrium conditions, such as In_2O_3 pyramids, octahedra, etc.[16–20] Recently, In_2O_3 nanocubes have been synthesized through hydrothermal and chemical vapor deposition (CVD) methods;[21–23] this kind of structure terminated with a high energy plane (100) is expected to have potential applications as a sensor. However, the relevant research on the dynamic growth mechanism for this kind cubic nanocrystal terminated with high energy planes has never been performed.

In this article, large-scale synthesis of In_2O_3 nanocubes was realized by modulating experimental parameters through the CVD method. Two contrastive experiments were performed to investigate the growth model of In_2O_3 nanocubes. The research results indicated that the formation of In_2O_3 nanocubes was the result of isotropic growth along three equivalent crystallographic directions [100], via a dynamic nonequilibrium process. The growth model was determined by two crucial growth factors: high reagent supersaturation ratio and relatively low growth temperature. The systemic research on the controlled growth of high energy planes was very significant, especially for the preparation of these functional nanostructures with special exposed crystallographic planes. Moreover, the synthesized In_2O_3 nanocubes may have important applications as sensors in the future microscale industry.

2. Experimental Section

The preparation of products was carried out in a conventional horizontal tube furnace with a 2-cm inner-diameter alumina tube mounted inside. In a typical experimental procedure, high purity 0.5 g metal indium particles (In, purity: 99.99%) with an average diameter of 0.5 mm was put into the alumina boat to serve as the source material. The boat was placed at the center of the alumina tube. The local temperature distribution in the tubular furnace has been calibrated in advance. A single-crystalline silicon wafer (1×1 cm^2) was put downstream to collect products (distance from the source: 13−14 cm, corresponding temperature range: 570−640 °C). Before heating, the tube chamber was purged with 200 sccm high purity N_2 (purity: 99.999%) for 10 min to clear the oxygen, and then 100 sccm argon (purity: 99.5) was introduced into the reaction chamber to serve as a carrying gas. The furnace was rapidly heated to 1000 °C in 10 min and kept at this temperature for 40 min. After the system was cooled to room temperature, a yellow powder layer was observed deposited on the silicon wafer.

The as-prepared products were characterized by X-ray diffraction (XRD) spectroscopy (Philips X'pert-PRO, Cu Kα (0.15419 nm radiation), field emission scanning electronic microscopy equipped with energy dispersive spectroscopy (SEM: Sirion 200 FEG), and high-resolution transmission electron microscopy (HRTEM, JEOL 2010, at 200 kV).

3. Results and Discussion

3.1. Structures and Characterization. Figure 1 showed the X-ray diffraction spectra of the obtained products. All the peaks could be indexed to body-centered cubic (bcc) In_2O_3 single crystal with a lattice constant of $a = 10.11$ Å (JCPDS card No. 06-0416). No other impurity phases, such as indium, were detected.

The morphology of the products was examined using FESEM. The low-magnification SEM image (Figure 2a) revealed that a large quantity of nanoscale particles with cubic configuration was deposited onto the Si substrate. The size of these nanocubes was in the range of 100−800 nm, and the average size was

* To whom correspondence should be addressed. E-mail: yyg@issp.ac.cn.
† China University of Petroleum.
‡ Key Laboratory of Materials Physics, Anhui Key Laboratory of Nanomaterials and Nanotechnology.

10.1021/cg800105h CCC: $40.75
Published on Web 07/23/2008

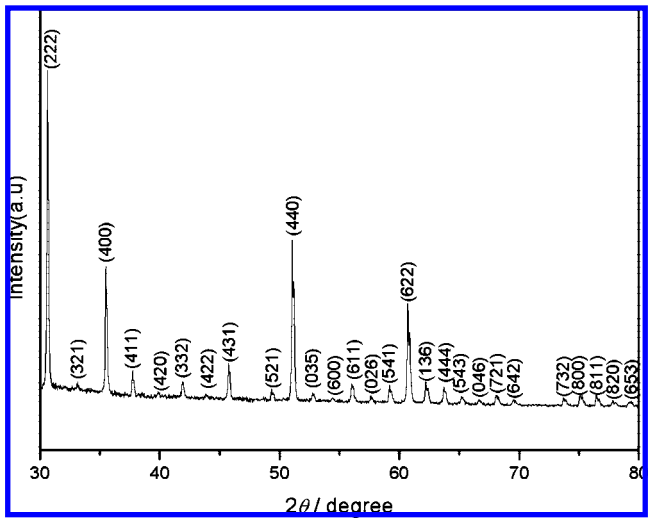

Figure 1. XRD pattern of prepared products deposited on the Si substrate.

about 300 nm. Figure 2b shows the magnified SEM image of these nanocubes. It can be seen that the obtained nanocubes were terminated with perfect equivalent crystallographic planes (100).

Further structural characterizations were performed with TEM as shown in Figure 3. Figure 3a gave the low-magnification TEM image of these In_2O_3 detected nanocubes with a small size of about 120 nm, which facilitated structure characterization using TEM. Figure 3b showed the high-resolution TEM (HRTEM) image of the area labeled with a white pane in Figure 3a. A magnified crystal lattice image and corresponding selected area electron diffraction (SAED) pattern are inserted in Figure 3b. The lattice image revealed that the spacing of two groups of crystallographic planes vertical to each other are all 0.506 nm, which corresponds to the (200) and (020) planes of bcc In_2O_3, respectively, and the SAED pattern results further validated the crystalline structure.

3.2. Growth Mechanism. 3.2.1. Dynamic Growth Model. In the growth of crystal, four sequential steps are involved:[24] (1) transportation of the reagent species in the vapor phase; (2) absorption of reagent species onto the surface of the nucleus; (3) transfer of absorbed species along the surface of nucleation; (4) precipitation, incorporation, and crystal growth. In this process, there are two crucial factors determining the growth behavior of crystal: mobility and mean free path of absorbed reagent species.[25,26] The mobility depended on the growth temperature, and under high temperature, the molecular kinetic energy was high and these absorbed species would have high mobility. As for the mean free path, which was determined by the supersaturation ratio, under a high supersaturation ratio, the opportunities of the absorbed species impinging on each other would increase and the mean free path would decrease.

In general, under dynamic equilibrium conditions, the reagent species would have high mobility and a large mean free path. The absorbed species would preferentially transfer to the high energy crystallographic planes and incorporate into the crystal lattice; these crystallographic planes would have a higher growth

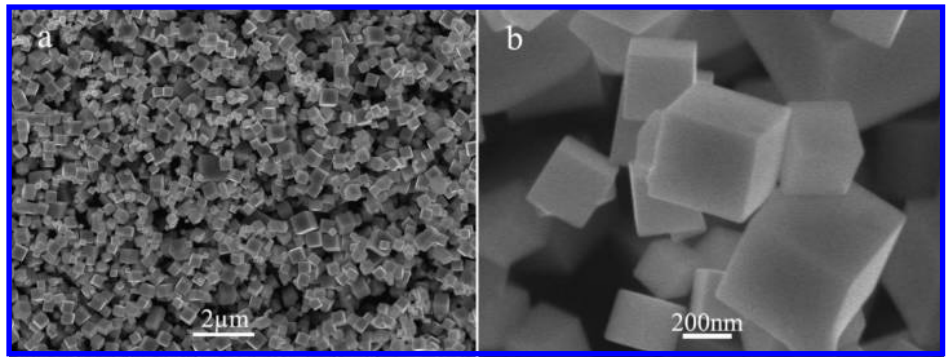

Figure 2. SEM image of obtained In_2O_3 nanocubes: (a) low-magnification and (b) high-magnification SEM images.

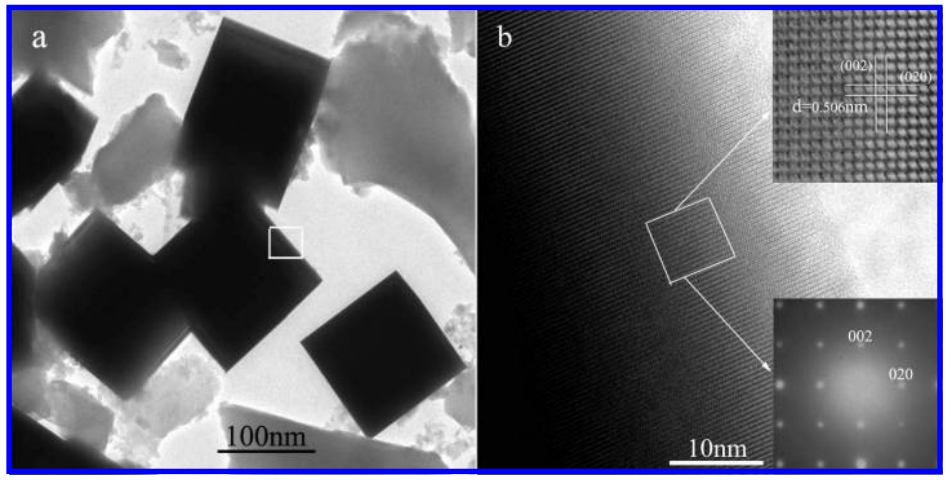

Figure 3. (a) TEM and (b) HRTEM images of typical nanocubes; the insets in panel (b) show the high-resolution crystal lattice image and corresponding SAED.

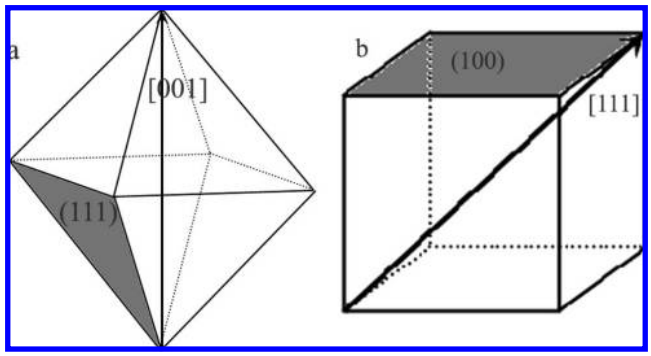

Figure 4. Crystallographic model of In_2O_3 octahedron and cube, (a) and (b) indicated the quickest growth crystallographic directions [100] and [111] in octahedron and cube, respectively.

rate than that of the low energy planes. The growth rate of low-index crystallographic planes was proportional to their surface energies. So, after growth, the high energy planes would preferentially disappear and the obtained crystal would be terminated with low energy planes.

For In_2O_3 with bcc structure, the surface energy relationships among three low-index crystallographic planes should correspond to $\gamma_{\{111\}} < \gamma_{\{100\}} < \gamma_{\{110\}}$,[27,28] so the growth rates of three growth directions had such relationships: $r_{<111>} < r_{<100>} < r_{<110>}$. Under dynamic equilibrium conditions, the grown In_2O_3 nanoparticles would be terminated with equivalent low energy planes (111) and possess octahedral configuration as shown in Figure 4a. In the octahedron, it can be seen that the growth ratio R, the growth rate in the <100> to that of the <111>, was about 1.73,[27] which indicated that the growth of the high energy plane (100) was the fastest. Figure 4b shows the configuration sketch map of a cube, and it can be seen that the fast growth direction was along <111>, while not <100> along the high energy plane, which revealed that the growth of cube occurred under nondynamic equilibrium conditions. At the same time, it could be seen that the growth rate along three equivalent crystallographic directions [100], [010], and [001] was uniform.

From the above analysis, the growth of cubes was conducted under nondynamic equilibrium conditions. As for In_2O_3, how did the In_2O_3 nanocubes grow? In order to recognize this point, two corresponding experiments were conducted from two aspects: growth temperature and supersaturation ratio, respectively.

3.2.2. Growth Temperature. As for the influence of the growth temperature, an experiment was conducted (defined as experiment I). Keeping all the experimental parameters unchanged, four similar cleaned Si wafers (1×1 cm^2, defined as Si−I, II, III, and IV) were placed downstream with a distance from the raw material of about 7−8, 10−11, 13−14, 16−17, and corresponding temperature: 860−890 °C, 750−790 °C, 570−640 °C, and 370−450 °C, respectively. After the reaction, four silicon wafers were observed with FESEM. Figure 5a−d shows the typical SEM images of deposited particles on four silicon wafers along the flow direction. Figure 5a shows the SEM image of deposited particles on Si−I. The size of the obtained octahedra was in the range of 1−1.5 μm, and the average size was about 1.2 μm. Figure 5b revealed that the deposited particles consisted of nanoscaled octahedra, truncated octahedra, cubes, and truncated cubes. The size was in the range of 300−800 nm with a mean value about 500 nm. The particles shown in Figure 5c were almost nanocubes mixed with a few truncated octahedra, and the size was in the range of 200−800 nm with an average value of about 350 nm. Figure 4d reveals that the obtained nanoparticles were imperfect nanocrystals without certain crystallographic planes possessing a uniform size about 200 nm. From above experimental results, it can be concluded that the configuration of grown particles underwent an evolution from octahedra to cubes with the decrease of the growth temperature.

In these experiments, a large flow rate (100 sccm) and small inner diameter (2 cm) of alumina tube was adopted, so the

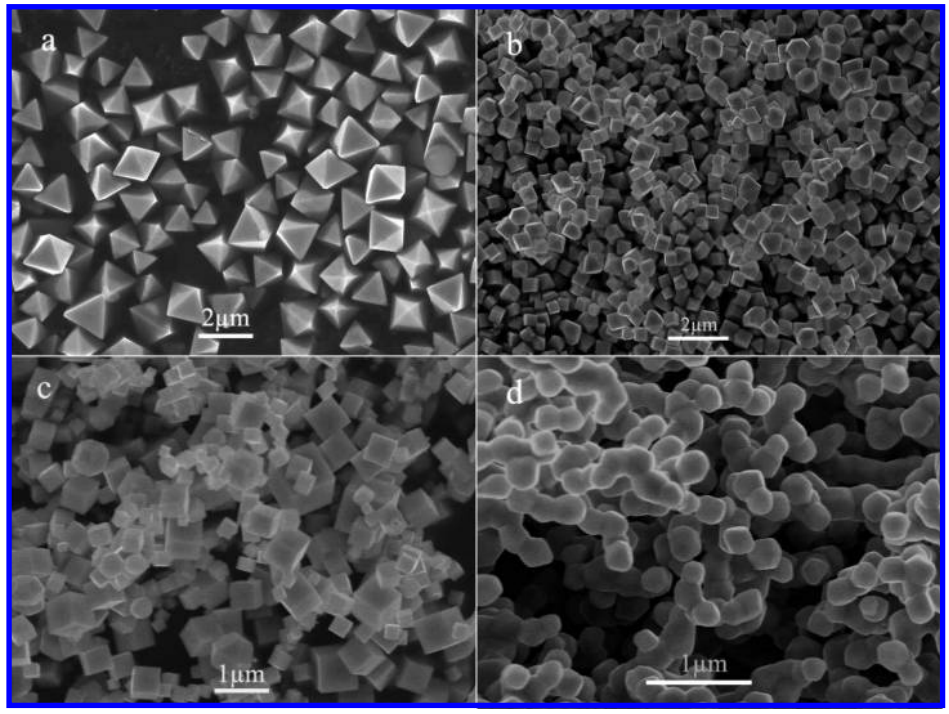

Figure 5. SEM images of In_2O_3 particles in experiment I (a−d) showed the SEM image deposited on four Si substrates (I−IV) respectively, revealing the morphology and size evolution orderliness of configuration.

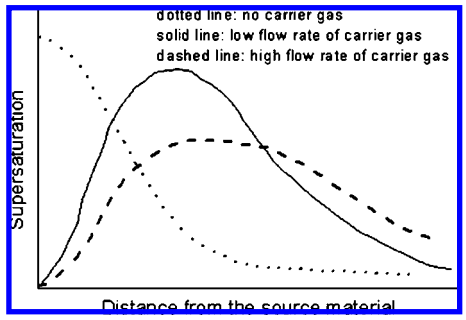

Figure 6. Reagent supersaturation distributing graph along the flow with a small Reynolds number in our experimental system.

Reynolds number in our experimental system was small. The transport of reagent species belonged to a passive convective process.[29,30] Figure 6 gives the distributing graph of reagent supersaturation under different fluxes of carrying gas in the reacting tube. In our experiment, the distinction of reagent supersaturation ratio along the flow direction was small because of the large flow rate (100 sccm). It indicated that the mean free path of reagent species upon four Si substrates was approximately the same. So the influence of supersaturation on the growth behavior was a secondary factor. Thus, the growth temperature resulted in the evolution of configuration.

From Si−I to IV, the growth temperature gradually decreased. Experimental results revealed that the growth of octahedra processed at a high temperature (860−890 °C), and meanwhile the growth of cubes was at a low temperature (570−640 °C). On the basis of the above the dynamic growth analysis, the configuration evolution could be interpreted as follows.

Under high temperature (Si−I), the reagent species with high mobility would have large opportunities transporting to a high energy plane, and the preferential growth of a high energy plane would lead to the formation of octahedra. With a decrease of the growth temperature from Si−I to IV, the mobility of the reagent species gradually decreased. As a result, the ratio of absorbed reagent species transferred to a high energy plane would decrease. On the other hand, the ratio of absorbed reagent species precipitated and incorporated into a crystal lattice would increase during transfer to the high energy planes, so the opportunities for isotropic growth along three equivalent directions [100] would increased. The deposited particles at Si−II (750−790 °C), viz. coexistence of octahedra, truncated octahedra, truncated cubes and cubes, were just the transitional stage from octahedra to cubes. When the growth temperature further decreased to 570−640 °C isotropic growth along three equivalent [100] directions was realized and nanocubes were obtained on the surface of Si−III. With a further decrease of the growth temperature (370−450 °C), from Figure 5d, it could be found that the deposited nanoparticle on Si−IV did not have certain crystallographic planes; the reagent species aggregated into semispherical nanocrystals.

From the above experimental results, it could be concluded that, in our experiment, the growth of In_2O_3 nanocubes was realized through isotropic growth along three equivalent crystallographic directions [100]. The synthesis could be realized only in an appropriate temperature range. A higher temperature induced to the formation of octahedra, while a lower temperature resulted in the formation of semispherical nanocrystals without certain crystallographic planes.

It is worth pointing out that that the size of obtained particles on four Si substrates also had definite orderliness. From high temperature (Si−I) to low temperature (Si−IV), the size of grown particles changed from 1.2 μm to 200 nm. The orderliness of size depending on the growth temperature may have an important reference in the controlled growth of functional nanodevices with special size demands.

3.2.3. Supersaturation Ratio. It is well-known that different materials have different supersaturation ratios under the same temperature. In order to investigate the effect of supersaturation ratio on the growth of In_2O_3 nanocubes, another comparative

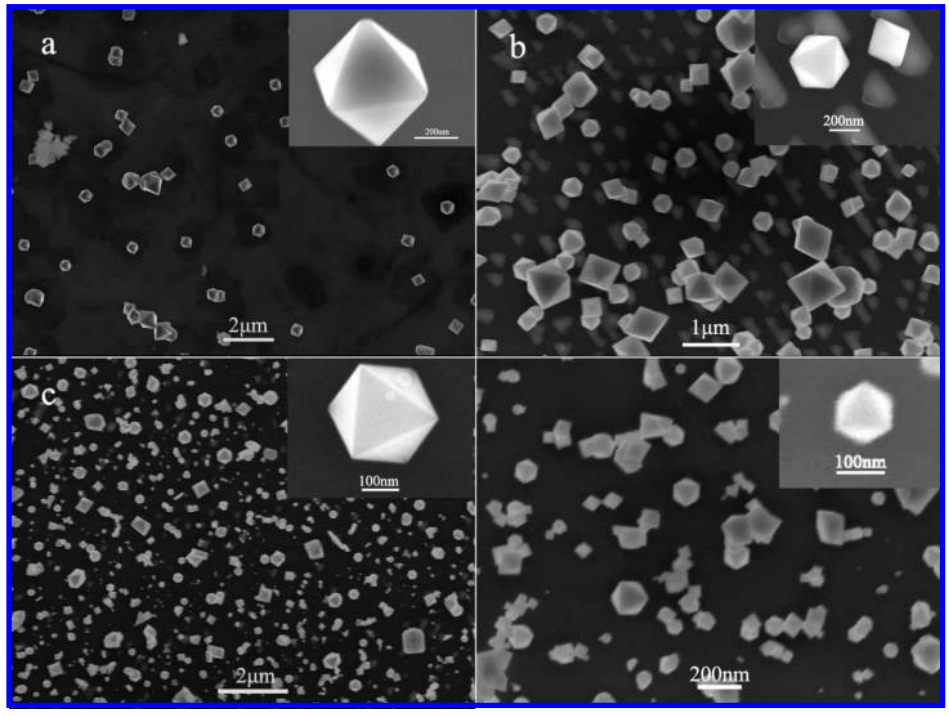

Figure 7. SEM images of In_2O_3 particles in experiment II (a−d) showed the SEM image of octahedral particles deposited on four Si substrates with different sizes, respectively.

experiment was conducted (defined as experiment II). Keeping other experimental conditions unchanged, a 0.5 g mixture of indium oxide and activated carbon powder (molar ratio = 1:3) was adopted as the source to replace metallic In particles. For metallic In particles, under 950 °C, the In vapor directly vaporized from the In metallic particles. However, for the mixture of indium oxide and activated carbon powder, the In vapor indirectly came from the carbothermal reduction reaction.[31] So the supersaturation of reagent species was lower in experiment II than in experiment I.

Figure 7 showed the SEM image of the obtained products. Figure 7a−d gave the typical SEM images of four silicon wafers along the flow direction. The results indicated that the deposited particles on four silicon wafers were all octahedra, but had different sizes. Similar to experiment I, there was the same changing orderliness of size among these deposited particles on four Si wafers, viz. with a decrease of depositing temperature (from Si−I to IV), the mean size gradually decreased from 470, 360, 260 to 120 nm.

In this experiment, the supersaturation of reagent species was lower than that of the In source. On the basis of the above dynamic growth analysis, under a lower supersaturation ratio, the reagent species possessed a larger mean free path, so the absorbed reagent species had more probability transferring to high energy planes, and the growth would induce the formation of octahedral configuration particles. Even at low temperatures at Si−IV, the large mean free path could impel these absorbed species to transfer to high energy planes and realize anisotropic growth along high energy planes under dynamic equilibrium conditions, so the obtained particle would maintain octahedral crystallographic configuration.

Thus, from these experimental results it could be seen that for the growth of reagent species processed under dynamic equilibrium conditions with low supersaturation ratios, the obtained In_2O_3 particles would be terminated with low-energy crystallographic planes (111) and had octahedral configuration. In order to obtain In_2O_3 nanocubes, a high supersaturation ratio was necessary, which would lead to a small mean free path and destroy the dynamic growth equilibrium condition. Under nondynamic growth equilibrium conditions, the reagent species could realize isotropic growth along three equivalent crystallographic directions [100], and obtain a cubic crystallographic structure.

4. Conclusion

In summary, In_2O_3 nanocubes were successfully synthesized by modulating experimental conditions. The In_2O_3 nanocube was terminated with three equivalent high energy crystallographic planes (100). The crystallographic configuration was determined by the growth rate of different low-energy crystallographic planes. Under dynamic equilibrium conditions, the growth rates of crystallographic planes were proportional to the surface energy, and octahedral particles terminated with equivalent low energy (111) planes would be obtained. For the formation of In_2O_3 nanocubes, the growth was determined by two growth parameters: low growth temperature and high supersaturation ratio. Under these experimental conditions, the reagent species would have low mobility and a small mean free path. The growth along three equivalent crystallographic directions [100] was isotropic, which destroyed the dynamic growth equilibrium and induced the formation of cubic particle.

The relevant research on the dynamic growth mechanism of In_2O_3 nanocubes is a significant exploration of the microcosmic growth behavior of nanoscale materials. The discussions about the growth of crystallographic planes are very important for the controlled growth of various functional nanodevices with special demands for crystallographic planes. Furthermore, the various obtained In_2O_3 nanoparticles including octahedra and cubes may have important potential applications, especially as chemical sensors.

Acknowledgment. This work was financially supported by the National Major Project of Fundamental Research: Nanomaterials and Nanostructures (Grant No. 2005CB23603), the Special Fund for President Scholarship, Chinese Academy of Sciences, and the National Natural Science Foundation of China (Grant No. 90406008).

References

(1) Shimizu, Y.; Egashira, M. *MRS Bull.* **1999**, *24*, 18.
(2) Williams, D. E. *Sens. Actuators B* **1999**, *57*, 1.
(3) Strassler, S.; Reis, A. *Sens. Actuators* **1983**, *4*, 465.
(4) Chung, W. Y.; Sakai, G.; Shimanoe, K.; Miura, N.; Lee, D. D.; Yamazoe, N. *Sens. Actuators B* **1998**, *46*, 139.
(5) Liess, M. *Thin Solid Films* **2002**, *40*, 183.
(6) Tamaki, J.; Naruo, C.; Yamanoto, Y.; Matsuoka, M. *Sens. Actuators B* **2002**, *83*, 19.
(7) Kiriakids, G.; Bender, M.; Kataarakis, N.; Gagaoudakis, E.; Hourdakis, E.; Douloufakis, E.; Cimalla, V. *Phys. Status Solidi A* **2001**, *185*, 27.
(8) Kong, J.; Franklin, N. R.; Zhou, C.; Chapline, M. G.; Peng, S.; Cho, K.; Dai, H. *Science* **2000**, *287*, 622.
(9) Kong, J. M.; Chapline, G.; Dai, H. *Adv. Mater.* **2001**, *13*, 1384.
(10) Law, M.; Kind, H.; Messer, B.; Kim, F.; Yang, P. *Angew. Chem., Int. Ed.* **2002**, *41*, 2405.
(11) Comini, E.; Faglia, G.; Sberveglieri, G.; Pan, Z.; Wang, Z. *Appl. Phys. Lett.* **2002**, *81*, 1869.
(12) Neri, G.; Bonavit, A.; Micali, G.; Rizzo, G.; Galvagno, S.; Niederberger, M.; Pinnac, N. *Chem. Commun.* **2005**, 6032.
(13) Li, C.; Zhang, D. H.; Liu, X. L.; Han, S.; Tang, T.; Han, n/a.; Zhou, C. W. *Appl. Phys. Lett.* **2003**, *82*, 1613.
(14) Zhang, D. H.; Li, C.; Liu, X. L.; Han, S.; Tang, T.; Zhou, C. W. *Appl. Phys. Lett.* **2003**, *83*, 1845.
(15) Zhang, D. H.; Liu, Z. Q.; Li, C.; Tang, T.; Liu, X. L.; Han, S.; Lei, B.; Zhou, C. W. *Nano Lett.* **2004**, *4*, 1919.
(16) Hsin, C. L.; He, J. H.; Chen, L. J. *Appl. Surf. Sci.* **2005**, *244*, 101.
(17) Guha, P.; Kar, S.; Chaudhuri, S. *Appl. Phys. Lett.* **2004**, *85*, 3851.
(18) Jia, H. B.; Zhang, Y.; Chen, X. H.; Shu, J.; Luo, X. H.; Zhang, Z. S.; Yu, D. P. *Appl. Phys. Lett.* **2003**, *82*, 3851.
(19) Hao, Y. F.; Meng, G. W.; Ye, C. H.; Zhang, L. D. *Cryst. Growth Des.* **2005**, *5*, 1617.
(20) Zhang, Y. J.; Ago, H.; Liu, J.; Yumura, M.; Uchid, K.; Ohshima, S.; Iijima, S.; Zhu, J.; Zhang, X. Z. *J. Cryst. Growth* **2004**, *264*, 363.
(21) Lee, C. H.; Kim, M.; Kim, T.; Kim, A.; Paek, J.; Lee, J. W.; Choi, S. Y.; Kim, K.; Park, J. B.; Lee, K. *J. Am. Chem. Soc.* **2006**, *128*, 9326.
(22) Tang, Q.; Zhou, W. J.; Zhang, W.; Qu, S. M.; Jiang, K.; Yu, W. C.; Qian, Y. T. *Cryst. Growth Des.* **2005**, *5*, 147.
(23) Shi, M. R.; Xu, F.; Yu, K.; Zhu, Z. Q.; Fang, J. H. *J. Phys. Chem. C* **2007**, *111*, 16267.
(24) Hao, Y. F.; Meng, G. W.; Wang, Z. L.; Ye, C. H.; Zhang, L. D. *Nano Lett.* **2006**, *6*, 1650.
(25) Hao, Y. F.; Meng, G. W.; Ye, C. H.; Zhang, X. R.; Zhang, L. D. *J. Phys. Chem. B* **2005**, *109*, 11204.
(26) Hao, Y. F.; Meng, G. W.; Zhang, L. D. *Nanotechnology* **2006**, *17*, 5006.
(27) Wang, Z. L. *J. Phys. Chem. B* **2000**, *104*, 1153.
(28) Yan, Y. G.; Zhang, Y.; Zeng, H. B.; Zhang, L. D. *Cryst. Growth Des.* **2007**, *7*, 940.
(29) Nam, C. Y.; Tham, D.; Fischer, J. E. *Appl. Phys. Lett.* **2004**, *85*, 5676.
(30) Brenner, S. S. *Acta. Met.* **1956**, *4*, 62.
(31) Yan, Y. G.; Zhang, Y.; Zeng, H. B.; Zhang, J. X.; Cao, X. L.; Zhang, L. D. *Nanotechnology* **2007**, *18*, 175601.

CG800105H